Acta Biomaterialia 121 (2021) 405–417

Contents lists available at ScienceDirect

Acta Biomaterialia

journal homepage: www.elsevier.com/locate/actbio

Human mesenchymal stem cell-engineered length scale dependent rheology of the pericellular region measured with bi-disperse multiple particle tracking microrheology

John A. McGlynn, Kilian J. Druggan, Kiera J. Croland, Kelly M. Schultz*

Department of Chemical and Biomolecular Engineering, Lehigh University, 111 Research Dr., Iacocca Hall, Bethlehem, PA 18015, USA

ARTICLE INFO

Article history:
Received 22 September 2020
Revised 25 November 2020
Accepted 27 November 2020
Available online 3 December 2020

Keywords:
Cell migration
Hydrogel
Multiple particle tracking microrheology
Cytoskeletal tension
Rheology

ABSTRACT

Biological materials have length scale dependent structure enabling complex cell-material interactions and driving cellular processes. Synthetic biomaterials are designed to mimic aspects of these biological materials for applications including enhancing cell delivery during wound healing. To mimic native microenvironments, we must understand how cells manipulate their surroundings over several length scales. Our work characterizes length scale dependent rheology in a well-established 3D cell culture platform for human mesenchymal stem cells (hMSCs). hMSCs re-engineer their microenvironment through matrix metalloproteinase (MMP) secretions and cytoskeletal tension. Remodeling occurs across length scales: MMPs degrade cross-links on nanometer scales resulting in micrometer-sized paths that hMSCs migrate through, eventually resulting in bulk scaffold degradation. We use multiple particle tracking microrheology (MPT) and bi-disperse MPT to characterize hMSC-mediated length scale dependent pericellular remodeling. MPT measures particle Brownian motion to calculate rheological properties. We use MPT to measure larger length scales with 4.5 μm particles. Bi-disperse MPT simultaneously measures two different length scales (0.5 and 2.0 μm). We measure that hMSCs preferentially remodel larger length scales measured as a higher mobility of larger particles. We inhibit cytoskeletal tension by inhibiting myosin-II and no longer measure this difference in particle mobility. This indicates that cytoskeletal tension is the source of cell-mediated length scale dependent rheological changes. Particle mobility correlates with cell speed across length scales, relating material rheology to cell behavior. These results quantify length scale dependent pericellular remodeling and provide insight into how these microenvironments can be designed into materials to direct cell behavior.

Statement of significance

Human mesenchymal stem cell (hMSC) remodeling is a complex process across many length scales: single cross-links break on the nanometer scale, cellular extensions pull material and degrade paths through the scaffold to enable motility on the micrometer scale and bulk scaffold degradation occurs on macroscopic scales. We measure length scale dependent rheology during cell-mediated remodeling of the pericellular region using bi-disperse MPT and MPT. Bi-disperse MPT uses two particle sizes to quantify rheological changes on multiple length scales in one measurement. We measure that cells preferentially re-engineer their microenvironment across length scales using enzymatic secretions and cytoskeletal tension. By characterizing evolving length scale dependent rheology, new materials can be designed which better mimic native tissue and instruct cell behavior.

1. Introduction

Native biological niches enable and direct cellular processes using both physical and chemical cues [1–5]. Physical cues include pore size, scaffold architecture and rheological properties. These

* Corresponding author.
E-mail address: kes513@lehigh.edu (K.M. Schultz).

https://doi.org/10.1016/j.actbio.2020.11.048
1742-7061/

physical features are inherently length scale dependent and provide complex rheology, which is critical for cell-material interactions [2,4,6–9]. During cell-material interactions, cells receive cues from their microenvironment. They then remodel this microenvironment during basic processes. This creates a feedback loop, which is essential for normal cellular functions, but can also be exploited to direct specific processes [2,6–14]. New materials that are being designed to harness cellular function and instruct cells using microenvironmental cues need to also incorporate length scale dependent rheology in their design. But, characterization of length scale dependent rheology, especially during cell-material interactions, has been difficult. The use of microrheological techniques to characterize spatio-temporal rheological changes in the pericellular region during cell-material interactions has led to new information about this feedback loop and the microenvironment cells create [6–9,11,15,16]. In this work, we build off of previous microrheological studies, which focused on a single length scale, and extend it to characterize rheological evolution across length scales providing new insight into cell-mediated re-engineering in response to microenvironmental cues.

Biological tissue is composed of a variety of complex components and length scales which signal cells [2–4,17,18]. For example, cartilage is abundant in the body and is a network of collagen fibrils (Order of magnitude (*OoM*) 10 nm in diameter) interspersed with aggregates of other proteoglycans, which form a complex matrix (*OoM* 100 nm spacing between fibrils) that enable cell migration within and through this network [18]. In natural implantable materials, reconstituted collagen matrices can be designed with specified pore sizes (*OoM* 10 μm^2) and rheology is controlled by both mesh size and the thickness of the gel sample (*OoM* 100 μm) [2,19]. Synthetic biomaterials take inspiration from these natural scaffolds with an added goal of designing microenvironments that can manipulate cellular processes [6,14,20–24].

Material properties such as stiffness, pore size and matrix composition are tuneable properties which have been shown to influence cell morphology, migration speed and lineage specification, among others, in synthetic hydrogel scaffolds [2,25–27]. One important biomaterial design consideration is the variety of length scales that cell-material interactions occur on. On macroscopic scales, bulk scaffold degradation occurs due to cell-secreted enzymes and cytoskeletal tension [10]. On microscopic scales, individual cells use cytoskeletal tension and enzymes called matrix metalloproteinases (MMPs) to degrade tracks within the material as they migrate several hundred microns [6]. On micrometer and nanometer scales, cells locally remodel their environment by enzymatically degrading individual cross-links and applying forces on the network prior to and during migration [6–9]. To harness and manipulate cellular processes, a well-defined microenvironment must be presented to encapsulated cells.

Our work uses a poly(ethylene glycol) (PEG)-peptide hydrogel scaffold to 3D encapsulate human mesenchymal stem cells (hMSCs) [6,14,20,28,29]. This scaffold is widely used as a 3D cell culture platform [6–11,14,20,28–31]. A key design feature of this scaffold is that it is degraded by cell-secreted MMPs [6,10,14,28,32,33]. This allows encapsulated hMSCs to degrade and remodel their microenvironment using MMPs prior to and during migration [28,32–34]. These enzymes break single cross-links (*OoM* 1 nm) using secreted and membrane-bound MMPs on cellular extensions (*OoM* 1 μm in diameter and 10 μm long) to degrade pathways through the local microenvironment [12,35]. In addition to enzymatic degradation, cells also pull on their surrounding material through the use of focal adhesions and the motor protein myosin-II [36,37]. hMSCs exert tension on the pericellular region and can displace large pieces of material impacting larger length scales in the pericellular region (*OoM* 10 – 100 μm). These two components of cell migration form the basis of cellular remodeling of the pericellular region across multiple length scales [12].

In this work, we characterize real-time hMSC-mediated length scale dependent changes in the pericellular region using multiple particle tracking microrheology (MPT) and bi-disperse MPT. MPT is a passive microrheological technique in which the Brownian motion of fluorescent particles embedded in a sample is measured [28,38–44]. Particle Brownian motion is related to material rheological properties by the Generalized Stokes-Einstein Relation (GSER) [38,40,41,44–46]. MPT is uniquely positioned to measure dynamic, local rheological changes around a migrating cell because of the small sample volumes required and local measurement of rheology using fluorescent microscopy. Due to these advantages, MPT has been previously used to measure structural and rheological changes in the pericellular region of cells migrating in hydrogels [6–9,15,16].

Previous work focused on characterization of the pericellular region during basic cellular processes including measuring cell-mediated remodeling prior to and during motility as well as the deposition of extracellular matrix (ECM) [6–9,11,15,16]. The work measuring cell-mediated remodeling during motility in PEG-peptide hydrogels showed that the hMSC creates an environment that enables spreading and attachment prior to motility through the secretion of enzymes and inhibitors, with cytoskeletal tension playing a minimal role [7–9,11]. Work by Hafner et al. also used MPT to measure the change in material properties during hMSC differentiation and quantify the change in rheology during deposition of ECM in 2D human umbilical vein endothelial cell culture [16]. While these studies provide vital new information about the rheology of the scaffold microenvironment, they use a single probe particle size to characterize rheological properties. Due to the complexity in cell-material interactions and the heterogeneity of the pericellular microenvironment, expanding MPT measurements to include multiple particle sizes to characterize multiple length scales, will provide additional information about the complex microenvironments cells create to enable basic processes. To quantify dynamic pericellular rheology on multiple length scales simultaneously, we use bi-disperse MPT [47]. This measurement technique uses the principles of MPT, but includes two different sized particles in a single sample, to simulatenously characterize multiple length scales.

In this work, we quantify changes in pericellular rheology around encapsulated hMSCs on three different length scales: 0.5, 2.0 and 4.5 μm. Bi-disperse MPT simultaneously measures 0.5 and 2.0 μm probe particle mobility and MPT measures 4.5 μm particle mobility in separate experiments. We measure significantly more remodeling on the larger measured length scales. We hypothesize that this is a result of the two strategies hMSCs use to remodel their microenvironments: (1) enzymatic degradation by cell-secreted MMPs and (2) cytoskeletal tension. Because inhibition of MMP activity results in little to no scaffold remodeling and motility [8], we measure pericellular remodeling around hMSCs which cannot apply tension by inhibiting myosin-II to determine the role of cytoskeletal tension on the remodeling of each length scale. We next investigate how cellular forces influence the trajectories of each particle size to determine if particles are being directed to where forces are applied. Finally, we correlate the rheological state of the material on each length scale with cell motility. Overall, this work shows that hMSCs preferentially remodel larger length scales using cytoskeletal tension. Understanding how length scale dependent rheology changes cell motility and other basic cellular processes will enable design of new instructive biomaterials that mimic microenvironments cells create. These new materials could spatially direct motility and enhance and manipulate other cellular processes to be used as implantable scaffolds to improve wound healing and tissue regeneration.

2. Materials and methods

2.1. Hydrogel composition

Hydrogels are photopolymerized from an aqueous precursor solution that includes the hydrogel backbone, MMP-degradable cross-linker, adhesion ligand and other components [6,9,20,31,48]. The hydrogel backbone molecules are 4-arm star PEG-norbornene ($f = 4$ where f is the number of reactive functional groups, 3 mM, $M_n = 20,000$ g mol^{-1}, Sigma-Aldrich). The peptide cross-linker (KCGPQG↓IWGQCK where ↓ designates the cleavage site, $f = 2$, 3.9 mM, $M_n = 1,305$ g mol^{-1}, Bachem) and cellular adhesion ligand, CRGDS ($f = 1$, 1 mM, $M_n = 594$ g mol^{-1}, American Peptide Inc.) are included in the precursor solution. The pH of the precursor is adjusted to 7 using NaOH (10 mM, Fisher scientific). Thiols in the cysteines in both the cross-linker and cellular adhesion ligand react with -enes on the backbone in a radically mediated step-growth reaction which forms a cross-linked gel structure [49]. This peptide cross-linker sequence is chosen because it is cleaved by most cell-secreted MMPs resulting in degradation, enabling cell migration [14,21,33]. The adhesion ligand is included to enable integrin binding, which is necessary for cell attachment and migration [6–9,31].

The ratio of thiol groups in the cross-linker and -ene groups in the backbone is 0.65 : 1, which controls the stiffness of the hydrogel [31]. This ratio produces a hydrogel with a similar stiffness to adipose tissue ($\approx$ 100 Pa) [31].

In addition to the gel components, the precursor solution also includes probe particles for microrheological measurements and hMSCs which are isotropically encapsulated during the gelation reaction. The hydrogel is cross-linked by exposing the precursor solution to UV light at 365 nm (5 mW/cm^2, Analytik Jena, UVP UVL-56) in the presence of a photoinitiator, lithium phenyl-2,4,6-trimethylbenzoylphosphinate (LAP, 1.7 mM). LAP is used because it is highly water soluble and not cytotoxic [10,20,48]. It is synthesized using previously published protocols [48]. Hydrogels cross-linked by step-growth polymerization have homogeneous structures and previous studies have shown that degradation by enzymes alone results in MPT measurements of homogeneous microenvironments during degradation. Heterogeneities will be present in the structure, but they are much smaller than the length scale measured by our probe particles [28,50].

2.2. Probe particles

Carboxylated fluorescent polystyrene probe particles (Polysciences, Inc.) of varying size are added to the precursor solution to enable microrheology measurements. The size of all particles used for these experiments are much larger than the native mesh size of the gel scaffold. This enables characterization of network properties [38,39,41,44]. All particles use the same yellow-green fluorophore with excitation and emission wavelengths of 441 and 486 nm, respectively. Bi-disperse MPT uses 0.5 μm ($2a = 0.49 \pm 0.01$ μm, where a is the particle radius, $C.V. = 3\%$ where $C.V.$ is the coefficient of variation in the diameter of the particle) and 2.0 μm ($2a = 2.00 \pm 0.08$ μm, $C.V. = 5\%$) particles. These particles are added to the same precursor solution for simultaneous length scale dependent rheological measurements at concentrations of 0.1% and 0.5% solids per volume for the 0.5 and 2.0 μm particles, respectively. This particle concentration is selected to balance having enough particles in the field of view for statistically significant MPT measurements and increasing particle separation distance to minimize particle-particle interactions.

Methoxy-PEG-amine molecules (mPEG-NH$_2$, $M_n = 750$ g mol^{-1}, Sigma-Aldrich) are covalently tethered to the surface of the 0.5 and 2.0 μm particles using a previously published procedure to prevent particle aggregation, which would invalidate microrheological measurements [51]. This size of PEG molecule is chosen for PEGylation because it does not significantly change the radius of the probe particles. From calculations, we estimate that the reaction conditions used provide enough PEG to fully cover the particle surface. Particles are PEGylated in a separate reaction and subsequent washing removes any potential contamination of the samples with PEGylation reaction components. PEGylated particles are measured in honey solutions and their diffusivity is calculated. We measure that PEGylated particles have the same diffusivity as bare particles of the same size. These results are provided in the Supplementary Material (Figure S12).

Separate MPT experiments use 4.5 μm ($2a = 4.30 \pm 0.27$ μm, $C.V. = 7\%$) particles at a concentration of 0.5% solids/volume. 4.5 μm particles did not aggregate and, therefore, PEG was not added to the surface of these particles.

The range of particle sizes is limited by the experimental apparatus and tracking algorithm. Particles smaller than 0.5 μm would be too small to accurately locate the brightness-weighted centroid of the particle with MPT tracking algorithms and particles larger than 4.5 μm sediment prior to encapsulation in the hydrogel scaffold [38,44,53]. Particle sizes are also selected due to their relevance in cell migration. Wolf et al. measured the affect of matrix pore size on cell migration in reconstituted collagen. They found that the pore size optimal for migration was $5 - 7$ μm in diameter and that pores smaller than 2 μm greatly impeded migration of T-blast cells [2].

All particles are prepared the same way for bi-disperse MPT and MPT experiments, regardless of size or surface chemistry. Prior to use in an experiment, particles are washed by repeated centrifugation (Eppendorf centrifuge 5424) and resuspension. 0.5 μm particles are centrifuged at 7,000 RPM for 5 min. 2.0 and 4.5 μm particles are centrifuged at 5,000 RPM for 5 min. After three washing cycles, particles are sonicated (Branson CPX1800) for at least 15 min to break up any aggregates which may have formed during washing cycles. Particles are then added to the precursor solution prior to polymerization at the concentrations specified above. Control experiments measure that the presence of particles in the gel scaffold does not have a significant effect on the elastic modulus or gel structure. The results for these experiments are provided in the Supplementary Material (Figure S13).

2.3. hMSC culture and encapsulation

hMSCs are purchased from Lonza in passage two. They are cultured in growth media at 37°C and 5% CO_2. Growth media is a mixture of low-glucose Dulbecco's modified Eagle Medium (DMEM, Life Technologies) and 10% fetal bovine serum (FBS, Life Technologies). 0.5 μg mL^{-1} Fungizone (Life Technologies), 50 U mL^{-1} penicillin/streptomycin (Life Technologies) and 1 ng mL^{-1} recombinant human fibroblast growth factor (hFGF, PeproTech) are added to the media. Cells grow to $\sim$ 90% confluency before being used for an experiment or passaged. hMSCs are encapsulated in a hydrogel scaffold after trypsinization from the cell culture plate (150 mm × 25 mm Treated Cell Culture Dish, Corning Inc.) and resuspension in media without hFGF. They are added to the precursor solution at a final concentration of 2×10^5 cells mL^{-1}. This low concentration is chosen to minimize cell-cell interactions in the hydrogel scaffold.

2.4. Hydrogel formation and hMSC treatments

17 μL of precursor solution is added to the center of the sample chamber inside a polydimethylsiloxane (PDMS) ring. Details of the sample chamber are provided in the next section. This small amount of hydrogel is used to enable 3D isotropic swelling of the

scaffold during incubation. The precursor solution is exposed to UV light (365 nm, 5 mW cm^{-2}, Analytik Jena, UVL-56) for 3 minutes. After photopolymerization, sample chambers are filled with 4 mL of growth media without hFGF and incubated at 5% CO_2 and 37°C (Eppendorf, Inc.). After 2 hours, media is replaced with media without hFGF containing either myosin-II inhibitor, (-)-blebbistatin (Sigma Aldrich) in DMSO (Life Technologies), or adding only DMSO to the media (control conditions). Control experiments done by the Leight group at Ohio State University show that blebbistatin has a minimal effect on the activity of cell-secreted MMPs [52]. The final concentrations of (-)-blebbistatin and DMSO in the hydrogel incubation media are 50 μM and 29 μM, respectively. The DMSO concentration is held constant for both myosin-II inhibited and control experiments. After replacing the media, hydrogels are incubated overnight prior to microrheological data collection.

2.5. Sample chamber fabrication

Hydrogels are prepared inside a PDMS ring attached to a glass-bottomed Petri dishes ($D = 35$ mm, MatTek Corporation). This sample chamber is used to reduce drift of probe particles and translation of the hydrogel during microrheological measurements [6–9,44]. PDMS is used to enable nutrient diffusion from the media into the sample chamber, to ensure high viability of encapsulated hMSCs. The inner PDMS ring is cut from a flat sheet of PDMS. The flat sheet of PDMS is made in a large Petri dish (150 × 50 mm, Falcon) by mixing cross-linking agent with silicone elastomer base at a 1 : 10 ratio, degassing and curing overnight at 65°C. A short ($h \approx 6$ mm) ring of PDMS with an inner diameter of 6 mm and outer diameter of 10 mm is cut from the sheet using biopsy punches (Integra Biosciences). The PDMS ring is attached to the glass-bottomed Petri dish using uncured PDMS and incubating at 65°C overnight. Dishes are sterilized with 70% ethanol in water prior to use in an experiment.

2.6. Multiple particle tracking microrheology and bi-disperse MPT

Multiple particle tracking microrheology (MPT) and bi-disperse MPT are passive microrheological techniques that characterize temporal and spatial rheological properties [39,41,43–46,53]. MPT has several advantages, including: measuring low moduli materials over a large frequency range, requiring small sample volumes, rapidly acquiring data and collecting data using imaging enabling spatial characterization in the field of view [39,41,43–46,53]. These advantages make microrheology ideal for characterizing the pericellular region. MPT also has limitations including a low upper measurable moduli limit ($G' < 4$ Pa) and only being able to quantify certain rheological properties when the criteria for the GSER are met [39,41,44]. These limitations are considered when designing the experiments done in this work. We do not quantify moduli using the GSER because cellular remodeling invalidates the assumption that particle motion is purely Brownian [41,43,44,46]. Although we cannot calculate the moduli, we can still characterize changes in the network structure and state of the material during cellular remodeling.

During an experiment, a cell is located and centered in the field of view, a circle of radius 80 μm. As the cell moves, the field of view remains the same. This defines the pericellular region characterized in each experiment.

Bi-disperse MPT data (simultaneous measurement of 0.5 μm and 2.0 μm particles) are collected on an inverted microscope (Zeiss Observer Z1, Carl Zeiss AG) with a 63× water immersion objective (N.A. 1.3, 1× optovar, Carl Zeiss AG). A 40× air immersion objective (N.A. 0.75, EC Plan-Neofluar, Carl Zeiss AG) is used for MPT experiments that use 4.5 μm particles. The magnification is lowered for the 4.5 μm particles so that the brightness of these particles does not saturate the image and prevent accurate particle tracking. The field of view analyzed for experiments using 4.5 μm particles is reduced to be the same as the field of view for the experiments using 0.5 and 2.0 μm particles to enable direct comparison. Although the 4.5 μm particle field of view is reduced, there are still enough particles included in the measurement to ensure statistically significant MPT measurements [38].

The microscope is equipped with an incubation chamber, enabling data to be collected at 37°C and 5% CO_2. 800 frame videos (≈ 30 s) of particle motion are collected using an exposure time of 1 ms and frame rate of 30 frames s^{-1} (1024 × 1024 pixels, Miro M120, Vision Research Inc.). These settings are used to minimize static and dynamic particle tracking errors for the 0.5 μm particles [54]. Static error for 2.0 and 4.5 μm particles are determined by immobilizing particles on a glass substrate in 1M NaCl in water. The immobilized particles are then tracked and the measured mean-squared displacement (MSD, $\langle \Delta r^2(\tau) \rangle$) is the static error. The static error is then subtracted from future measurements. Static error is quantified for these particles because it is more significant than dynamic error. After data collection, particles are tracked using particle tracking algorithms [53,55].

For MPT experiments, particle positions are identified from the brightness-weighted centroid [38,44,53,55]. Each particle's brightness profile covers multiple pixels allowing us to distinguish differently sized particles in bi-disperse MPT measurements [44,47]. After particle positions are identified in each frame of the video, a probability distribution function is used to link particles through the frames in the video into trajectories [38,44,53,55]. These data are then used to calculate an ensemble-averaged mean-squared displacement (MSD, $\langle \Delta r^2(\tau) \rangle$). The measured MSD is a measure of particle mobility and defined as $\langle \Delta r^2(\tau) \rangle = \langle \Delta x^2(\tau) \rangle + \langle \Delta y^2(\tau) \rangle$. The logarithmic slope of the MSD, $\alpha = \frac{d \log \langle \Delta r^2(\tau) \rangle}{d \log \tau}$, is a measure of the state of the material [38,39,44]. Since the conditions in these experiments invalidate the GSER, including cells pulling on material, we use α to determine the state of the material and quantify particle mobility on each length scale [41]. $\alpha = 1$ indicates that particles are freely diffusing in a liquid and $\alpha = 0$ is when particles are arrested in a gel scaffold. $0 < \alpha < 1$ occurs in a viscoelastic sol or gel with the transition occuring when $\alpha = n$ where n is the critical relaxation exponent. $\alpha > n$ indicates a viscoelastic sol while $\alpha < n$ occurs in a viscoelastic gel [7,8,38,39,44]. We determine n for our material on each length scale, as described in the Results and Discussion.

For bi-disperse MPT, particles are tracked using the brightness-weighted centroid as described above. An additional step which uses a calculated radius of gyration based on the "weight" of the brightness of each pixel and the total brightness of all pixels in the particle is included to group particles by their size using the squared radius of gyration, R_g^2, defined as

$$R_g^2 = \frac{I}{B} \tag{1}$$

where I is the moment of inertia of the particle and B is a weight corresponding to the sum total of the brightness of the pixels of the particle [47]. I is defined by

$$I = \sum \left(b_i \times \left(r_i^2 + \frac{1}{6} \right) \right) \tag{2}$$

where b_i is the brightness of a pixel a distance r_i from the brightness-weighted centroid of the particle. The 1/6 term is added because a particle is approximated as a collection of square prisms (pixels) which have a moment of inertia of 1/6 [47,55]. This allows the tracking algorithm to identify particles separately by their size. Once a single particle size is tracked, their positions are linked into trajectories as described above and an ensemble-averaged MSD is calculated. This is repeated twice on a single

movie to track each particle size separately enabling rheological characterization as a function of probe particle size.

Prior to characterization of the pericellular region, bi-disperse MPT is used to characterize degradation of a PEG-norbornene hydrogel in the absence of cells at 37°C using collagenase. The average mesh size of our hydrogel network is on the order of 10 nm which is several orders of magnitude smaller than the size of particles used. This means that any particle motion measured is due to enzymatic degradation during collagenase experiments or cellular remodeling during cellular experiments. The collagenase degradation experiments determine the critical relaxation exponent, n, at both length scales. A more in-depth discussion of n is provided in the Results and Discussion and the Supplementary Material. Briefly, a hydrogel without cells is made with 0.5 and 2.0 μm particles. The gel is incubated in collagenase (0.5 mg/mL, Fisher Bioreagents). Collagenase is a mixture of enzymes secreted by *Clostridium histolyticum* which uniformly breaks the MMP-degradable cross-linker in our scaffold resulting in gel degradation [10,28]. Every $3-5$ minutes, a video is collected of particle motion using fluorescence microscopy for at least 2 hours to ensure the gel is completely degraded. Data are collected in 4 hydrogels made from 4 different stock solutions to ensure reproducibility.

Data for cell experiments are collected $18-72$ hours after hMSC encapsulation. Hydrogels are fully swollen after incubation in media for 4 hours, removing the impact of hydration state on the measurements [10]. All cell-laden hydrogels are incubated in media at 37°C and 5% CO_2 throughout the entire experiment, including during data acquisition. Upon finding a cell in the hydrogel, a brightfield image is taken to record the position of the cell which is used to calculate cell velocity. The time this picture is taken is $t = 0$ min. Immediately after taking the brightfield image, a video is collected using fluorescence microscopy to capture particle motion in the pericellular region. This process is repeated every $4-8$ minutes for up to 1 hour, or until the cell has gone out of focus or left the field of view. Data collection is limited to an hour due to photobleaching of probe particles in the pericellular region.

To measure spatial changes in the material around an encapsulated cell, particles in different non-overlapping regions are characterized separately. Each region is a concentric ring centered on the cell center with outer radius R. The first region is a circle with a radius $R_1 = 23.4$ μm (150 pixels). The next region is a ring with inner diameter $R_1 = 23.4$ μm and outer diameter $R_2 = 46.8$ μm. Each subsequent ring's outer radius is determined by $R_{i+1} = R_i +$ 23.4 μm and the inner radius is $R_{i+1} = R_i$. The width of the ring is chosen such that each region contains enough particles to ensure statistical significance of the MPT measurements. If a particle moves from one ring to another, the data will stop being recorded in the first ring and start being recorded in the second.

2.7. Cell speed and cell center determination

The center of mass of the cell is estimated from brightfield images using ImageJ (NIH Image). These points are used to calculate a cell velocity between consecutive time points,

$$v_{cell} = \frac{\sqrt{\left(x_f - x_0\right)^2 + \left(y_f - y_0\right)^2}}{t_f - t_0} \tag{3}$$

where (x_0, y_0) is the position of the cell at a given time, t_0, and (x_f, y_f) is the position of the cell at a later time, t_f.

2.8. Data analysis and statistics

Statistical significance is determined by a heteroscedastic t-test for Fig. 3. In Figs. 4 and 6 statistical significance is determined using a two-sample Kolmogorov-Smirnov (KS) test. We use the KS test to determine statistical significance in Figs. 4 and 6 because they do not have Gaussian distributions (an assumption in the heteroscedastic t-test) and because it is more sensitive to changes in shape of the distribution [56]. In Fig. 7 statistically significant differences between the slopes of each correlation are determined from analysis of variance (ANOVA). The difference and standard error in each fit are used to calculate a t-statistic which is then used to calculate a p-value. Distributions shown in Figs. 4, 5 and 6 are calculated by using a kernel density function. This is done to avoid assumptions about the shape of the distribution or the bin sizes and placements.

Bi-disperse MPT data are taken around 72 total cells, 37 are untreated and 35 are treated with blebbistatin. In a single pericellular region, data are collected temporally for an average of 35 min (526 temporal samples for 0.5 and 2.0 μm particles). 21 cells are measured on day 1: 10 treated with blebbistatin and 11 untreated. 28 cells are measured on day 2: 14 treated and 14 untreated. 23 cells are measured on day 3: 11 treated and 12 untreated. MPT measurements using 4.5 μm particles are taken for 80 total cells, 40 are untreated and 40 are treated with blebbistatin. In a single pericellular region, data are collected temporally for an average of 55 min (897 temporal samples for 4.5 μm particles). The increased data collection time for cells with 4.5 μm particles is due to the lower magnification objective used, which samples a larger space that cells remain in for longer times. 31 cells are measured on day 1: 16 untreated and 15 treated. 32 cells are measured on day 2: 15 untreated and 17 treated. 17 cells are measured on day 3: 9 untreated and 8 treated. By day 3, there is a significant loss of 4.5 μm particles due to gravitational sedimentation and the measurement is biased towards lower particle mobilities for the remaining 4.5 μm particles so less data are collected for 4.5 μm particles on day 3.

3. Results and discussion

In this work, we characterize remodeling in the pericellular region using bi-disperse multiple particle tracking microrheology (MPT) (simultaneous measurement with 0.5 and 2.0 μm particles) and MPT (4.5 μm particles). We begin by characterizing the temporal changes in the pericellular region around 3D encapsulated hMSCs. These measurements indicate that larger length scales are remodeled more than the 0.5 μm length scale. We hypothesize that this is due to enzymatic degradation by secreted MMPs and cytoskeletal tension applied to the network. Previous work indicated that MMP inhibition results in no pericellular remodeling or motility [8]. Therefore, bi-disperse MPT and MPT are used to measure the pericellular region around untreated hMSCs and hMSCs that cannot pull on the network due to myosin-II inhibition to determine the role of tension in scaffold remodeling. We correlate the measured rheology with cell speed, relating pericellular remodeling to basic cellular processes. Characterizing the microenvironments cells create during basic processes will enable design of new implantable materials that mimic these microenvironments to manipulate cell behavior to enhance wound healing and tissue regeneration.

Prior to characterization of cell-laden scaffold remodeling, the gel-sol transition must be measured. The critical relaxation exponent, n, identifies the gel-sol transition and is measured with bi-disperse MPT during isotropic hydrogel degradation in the absence of cells using collagenase [28,57]. n is a material property and will only be changed if the degradation reaction mechanism or structure (i.e. size of the polymer or cross-linker) of the material changes [38,58–62]. n has been previously determined for this material using MPT with 1.0 μm particles, $n = 0.25 \pm 0.05$ [6–8,28]. This low value of n ($n < 0.5$) indicates that this scaffold has a densely cross-linked structure. In our degradation experiments, we use bi-disperse MPT with the goal of determining whether

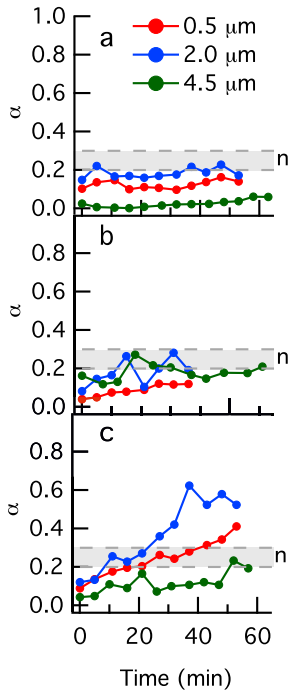

Fig. 1. Rheological state in the pericellular region around untreated hMSCs measured with bi-disperse MPT and MPT. Data are shown for (a) 1, (b) 2 and (c) 3 days post-encapsulation. Each line shows the change in $\alpha = \frac{d\log\langle\Delta r^2(\tau)\rangle}{d\log\tau}$ through time of a single pericellular region. Color represents the probe particle size. All data are representative of measurements taken on the specified day. Bi-disperse MPT measures the same field of view with 0.5 and 2.0 μm particles and MPT measures pericellular region with 4.5 μm particles. The shaded gray area is the gel-sol transition region ($n = 0.25 \pm 0.05$).

isotropic degradation of this material with collagenase is length scale dependent, which would result in a different value of n. Bi-disperse MPT measures $n = 0.17 \pm 0.08$ and $n = 0.23 \pm 0.08$ for 0.5 and 2.0 μm particles, respectively. These values are within error of one another and agree well with previously reported values. From these measurements, we conclude that the evolving rheology during the gel-sol phase transition of this network is not length scale dependent and the same critical phase transition point is measured regardless of particle size.

Once n is determined, we can characterize cell-mediated degradation. Fig. 1 shows representative data of the change in α over time, with $t = 0$ min being the time data acquisition is begun. Each line is the measurement of the pericellular region around a single cell and the color of the line represents the particle size used for the measurement. Representative data was selected by plotting the data for all cells and selecting one which was representative of the data set. These plots show differences in remodeling on each length scale in pericellular regions around untreated hMSCs on days 1 (Fig. 1a), 2 (Fig. 1b) and 3 (Fig. 1c) post-encapsulation. As hMSCs remodel their network, the α value of the pericellular region increases with time, indicating that particle mobility is increasing and the scaffold is being degraded. To determine the state of the material α is compared to n [44,60,63]. If $\alpha < n$ the material is a gel with a sample-spanning network. If $\alpha > n$ the material is a sol with no sample-spanning network structure. In Fig. 1, the gel-sol transition region is represented by a gray shaded area. On later days post-encapsulation, higher α values are measured because cells have had more time to remodel and degrade the surrounding scaffold.

Fig. 1a shows representative data 1 day post-encapsulation. We measure higher α values for 2.0 μm particles than 0.5 μm particles around untreated cells indicating that the larger length scale measured by the 2.0 μm particles is remodeled more and enters the gel-sol transition region. The 4.5 μm α value remains low because these particles are much larger and their mobility is inhibited by the surrounding network. On day 2 (Fig. 1b), we measure similar particle mobility for 0.5 and 2.0 μm particles as on day 1. The 4.5 μm particles have increased mobility relative to day 1 as cell-mediated scaffold degradation has broken more cross-links which previously had restricted the mobility of these larger particles. Finally by day 3 (Fig. 1c), we measure the most significant remodeling of the pericellular region on the 0.5 and 2.0 μm length scales. 2.0 μm particles continue to be more mobile than 0.5 μm particles but both measure that the material has been degraded to a sol. The α values for the 4.5 μm particles are low on this day. This is likely due to 4.5 μm particles that were in degraded areas of the hydrogel settling out of the material under gravity. Therefore, 4.5 μm particles available for MPT measurements are trapped in the remaining gel structure that has not been remodeled by encapsulated hMSCs. Additional data for cellular degradation is provided in the Supplementary Material (Figure S1).

Fig. 1 shows how hMSCs remodel different length scales in the material. The increased remodeling of larger length scales is counterintuitive. For example, in a Newtonian fluid smaller particles would have a higher diffusivity than larger particles. Additionally, in this hydrogel scaffold during enzymatic degradation in the absence of cells we measure 0.5 μm particles have higher mobility than 2.0 μm particles when the scaffold has completely degraded. We hypothesize that encapsulated hMSCs are preferentially remodeling larger length scales in the material prior to and during motility.

The α values plotted in Fig. 1a-c, are the α value from the ensemble-averaged MSD for the entire field of view (approximately $30 - 100$ particles). Previous work has shown that α varies significantly as a function of distance from the cell center [6–9]. Additionally, cytoskeletal tension will cause local remodeling and likely has a more significant impact on regions closer to the cell center due to the length scale of cellular extensions that apply this tension. To investigate cell-mediated changes in rheology as a function of distance from the cell center, we separate the pericellular region into different spatial rings and quantitatively identify the state of the material, reported as α, in each ring.

Fig. 2 is a spatio-temporal map of the rheological properties of the pericellular region around an untreated hMSC measured with bi-disperse MPT. This is representative data and additional plots of pericellular regions are provided in the Supplementary Material, Figures S2-4. In Fig. 2, a brightfield image of the cell is in the background and in the foreground are a series of colored rings. The color of each ring represents the α value of the particles within that ring. This divides the field of view into a series of regions that are distance R from the cell center. Warm colors represent low α values corresponding to a gel $\alpha < 0.2$. Conversely, cool colors represent higher α values where the material is a sol $\alpha > 0.3$. The gel-sol transition region is represented by orange colors ($0.2 \leq \alpha \leq 0.3$). Black rings are rings which do not have sufficient particles within the region for an accurate measurement of the MSD.

At the start of data acquisition around a hMSC on day 1 post-encapsulation ($t = 0$ min, Fig. 2a and b), we measure all rings have low α values on both the 0.5 and 2.0 μm length scales indicating that probe particles are arrested in a gel network where little to no cell-mediated degradation has occurred. At $t = 15$ min, we measure little to no degradation on the 0.5 μm length scale, $\alpha_{0.5\,\mu m} \approx 0$, and higher α values on the 2.0 μm length scale, $\alpha_{2.0\,\mu m} \geq 0.2$, Fig. 2c and d, respectively. This indicates that the scaffold is being degraded and remodeled on the 2.0 μm length scale and has reached the gel-sol transition region, $0.2 \leq \alpha \leq 0.3$. At 35 min, Fig. 2e and f, we measure a large increase in $\alpha_{2.0\,\mu m}$ while $\alpha_{0.5\,\mu m}$ remains at values below or in the gel-sol transition region. On the

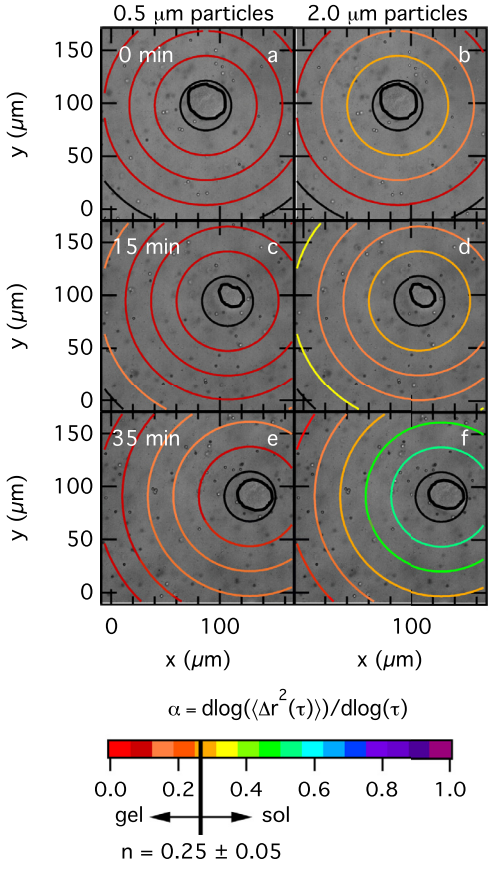

Fig. 2. Spatial degradation profiles in a single pericellular region around an untreated hMSC measured with bi-disperse MPT. These profiles use simultaneous measurements from (a, c and e) 0.5 and (b, d and f) 2.0 μm particles. Each row is a single time measurement, the time bi-disperse MPT measurements begin is 0 min. Rings divide the field of view into regions a distance R from the cell center to quantify spatial rheological changes. The color of each ring represents the α value for particles within that ring. This value indicates the state of the material with warm colors indicating a viscoelastic gel state and cool colors indicating a viscoelastic sol state. The transition region is $0.2 \leq \alpha \leq 0.3$ and is represented by orange colors. Degradation profiles are shown at (a and b) 0, (c and d) 15 and (e and f) 35 min. (a and b) At 0 min the material is a gel around the cell on both length scales. (c and d) At 15 min more degradation is measured on the 2.0 μm length scale than on the 0.5 μm scale, which continues at (e and f) 35 min.

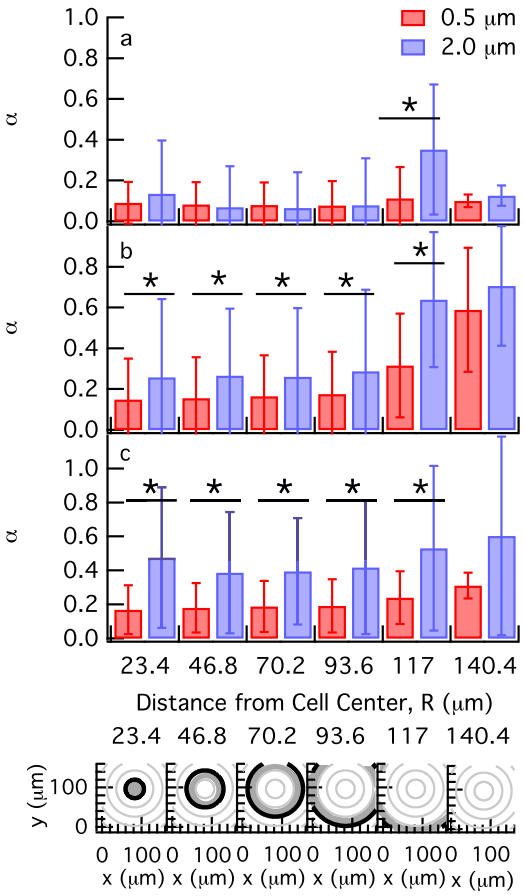

Fig. 3. Average α value for all pericellular regions around untreated hMSCs at various distances from the cell center (a) 1, (b) 2 and (c) 3 days post-encapsulation. The distance from the cell center R is shown at the bottom of the figure. Data are represented as an average across multiple experiments with standard deviation represented by the error bar. $*: p < 0.05$.

2.0 μm scale, material immediately around the cell center has transitioned from a gel to a sol. The difference in $\alpha_{0.5\,\mu m}$ and $\alpha_{2.0\,\mu m}$ is apparent in this map of the pericellular region, but this is only a single measurement. Therefore, we compare measurements on both length scales for all pericellular regions characterized with bi-disperse MPT.

Fig. 3 plots the average α value at each distance R from the cell center with error bars representing the standard deviation. Data are organized by the post-encapsulation day and all cell measurements and times for a single cell measurement are combined based on their distance from the cell center, R. On day 1 post-encapsulation, Fig. 3a, we measure low α values because hMSCs have not had sufficient time to degrade the material. This results in the same α values for each particle size as a function of R with the only significantly different value at $R = 117$ μm. Previous work in the same hydrogel scaffold measures the greatest degradation around an encapsulated hMSC at $R = 117$ μm on the 1 μm length scale [7–9]. Although these results seem to match with our measurement, scaffold degradation alone would not account for 2.0 μm particles having higher mobility than 0.5 μm particles in this region. This contributes to the hypothesis that the degradation strategy hMSCs are using is preferentially remodeling the 2.0 μm length scale more than the 0.5 μm length scale.

On day 2 post-encapsulation, Fig. 3b, we measure that α values increase compared to day 1. hMSCs have had more time to remodel the material and the cumulative effect of this remodeling on the network results in more mobile particles and higher α values. $\alpha_{2.0\,\mu m}$ is significantly higher than $\alpha_{0.5\,\mu m}$ at all distances from the cell center except the farthest region from the cell center, $R = 140.4$ μm. The lack of significance in the furthest region from the cell center is due to a low number of measurements in this region. In order for this region to be measured, the cell must move towards the edge of the field of view during data acquisition. This does not occur in all cells and, therefore, the number of measurements made in this region is small. Day 3 postencapsulation, Fig. 3c, provides similar trends to day 2, but the α values increase further. We also measure a larger α value for 2.0 μm particles in all but the farthest region from the cell center on this day.

The difference in the α values shown in Fig. 2 and 3 between the 0.5 and 2.0 μm particles is unexpected given: (1) diffusivity predicts smaller particles will move more than larger particles, (2) scaffold degradation generally proceeds by the degradation of single cross-links to larger structures, which would be measured by smaller particles before larger particles and (3) the results from our collagenase degradation experiments where $\alpha_{0.5\,\mu m}$ is always equal to or greater than $\alpha_{2.0\mu m}$. We also measure n values for both particles sizes that are within error of each other indicating that the phase transition happens at the same point and with the same

structure regardless of length scale. The collagenase degradation experiments indicate that enzymatic degradation will not result in length scale dependent rheological properties during scaffold degradation, but hMSCs remodel the pericellular region using both MMP-secreted enzymatic degradation and cytoskeletal tension.

As cell-secreted MMPs break cross-links, the material can also be moved by cytoskeletal tension. We hypothesize that the difference in mobility of 0.5 and 2.0 μm particles is due to cytoskeletal tension. Cellular extensions reach into a region and attach to material where they can then exert tension to enable migration. These extensions remodel larger length scales in the material, which results in a scaffold with a pore structure which does not restrict migration [2]. In bi-disperse MPT, we hypothesize that 2.0 μm particles are trapped in a pore structure of similar length scale and are measuring the movement of the scaffold when tension is applied. If the pore size is on the order of a few microns, the 0.5 μm particles are able to diffuse within this pore structure and this increased mobility is not measured. In order to test this hypothesis, we compare measured cell-mediated scaffold degradation around untreated and myosin-II, which applies cytoskeletal tension, inhibited hMSCs [64,65].

In order to quantify the difference in α we define a new parameter, $\Delta\alpha$, defined as

$$\Delta\alpha = \alpha_{2.0\mu m} - \alpha_{0.5\mu m}. \quad (4)$$

$\Delta\alpha$ quantifies relative changes in particle mobility and differences in scaffold structure based on length scale. Materials with the same microstructure on both length scales will have the same value of α, leading to $\Delta\alpha \approx 0$. $\Delta\alpha \approx 0$ is measured in a Newtonian fluid, Figure S5. Samples with more degraded larger length scales will have more mobile larger particles resulting in $\Delta\alpha > 0$. Similarly, materials with less structure on smaller scales will result in $\Delta\alpha < 0$ because the motion of the larger particles is hindered while smaller particles can move more freely. Fig. 4a-c is the distribution of $\Delta\alpha$ for pericellular regions around both untreated and myosin-II inhibited hMSCs measured with bi-disperse MPT. Using all data of measured particle motion in each region R, identified in the inset in Figs. 4a-c, for the same cell treatment a kernel smoothing function is used to calculate the probability density. Additional $\Delta\alpha$ distributions for $R > 70.2$ μm are provided in the Supplementary Material, Figure S6.

In Fig. 4a-c, pericellular regions around untreated hMSCs have distributions of $\Delta\alpha$ that are skewed towards positive values. This indicates that 2.0 μm particles are more mobile than 0.5 μm particles and the material is more remodeled on the 2.0 μm length scale. The $\Delta\alpha$ value in pericellular regions around myosin-II inhibited hMSCs show particle mobility is roughly the same for 0.5 and 2.0 μm particles and the distribution is centered around $\Delta\alpha \approx 0$. These measurements indicate that cytoskeletal tension is the cause for the positive skewness in $\Delta\alpha$. $\Delta\alpha$ distributions around untreated and myosin-II inhibited hMSCs are also statistically significant in regions nearest the cell shown in Fig. 4a-c. Cellular forces are applied in the region nearest the cell (Fig. 4a) and material is displaced further away from the cell center due to tension (Fig. 4b and c). When hMSCs apply force to the network, we hypothesize that the larger 2.0 μm particles are trapped in the pores of the partially degraded network and are pulled with the network. Since the scaffold has degraded, the smaller 0.5 μm particles still have hindered mobility but are not trapped in the pore structure and can roll through pores resulting in a measurement of limited particle motion. To determine whether this is a probable explanation for the difference in particle mobilities, we calculate whether 2.0 μm particles are directed towards force centers during our measurements.

To identify force centers within a sample we use the following steps: (1) calculate the representative particle vector using all displacements in a particle trajectory and repeat this for all particles of a given size in a sample, (2) extend each particle vector to the edge of the field of view to determine the long term movement of the particle and (3) identify the nearest locations where extended particle vectors intersect. Regions which have a high concentration of intersections are force centers. If particles are undergoing Brownian motion, there will be minimal force centers identified in the sample.

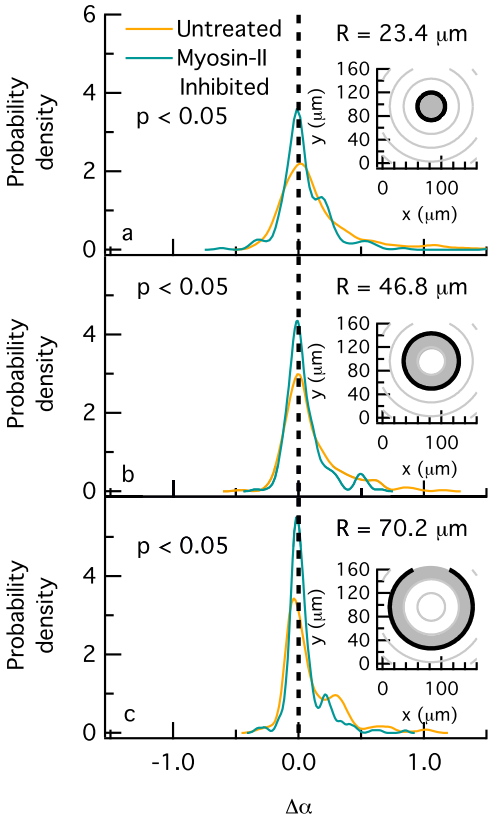

Fig. 4. Histograms of $\Delta\alpha$ values at various distances from the cell R for pericellular regions around both untreated and myosin-II inhibited hMSCs. Data are shown for regions (a) 23.4, (b) 46.8 and (c) 70.2 μm from the cell center. The inset for each plot shows the region around the cell where data are collected. Distributions that are centered indicate no difference between the measurements by 0.5 and 2.0 μm particles. Distributions skewed to the right indicate 2.0 μm particles have greater mobility and distributions skewed to the left indicate 0.5 μm particles have greater mobility. The untreated and myosin-II inhibited distributions are all significantly different from one another with $p < 0.05$.

An average particle vector is calculated using both x and y components. The x component of the vector, $\overline{\Delta x_i}$, is calculated using

$$\overline{\Delta x_i} = \sum_{\tau=0.033\ s}^{\tau_{max}} \frac{x|_\tau - x|_0}{\tau} \quad (5)$$

where τ_{max} is the duration the particle is in frame, $x|_0$ is the initial position of the particle and $x|_\tau$ is the position of the particle τ seconds later. All measurements begin at the first frame when the particle is located. The y component, $\overline{\Delta y_i}$, is calculated the same way using y coordinates of the particle positions. The calculated vector, $(\overline{\Delta x_i}, \overline{\Delta y_i})$, for each particle is then extended from the initial particle location to the edge of the field of view. This is done to project the particle motion beyond what is captured in our limited data acquisition time of ≈ 30 s. After particle vectors are extended, intersections of vectors are identified. Since probe particles can leave the field of view and re-enter and can be assigned a new particle number depending on the time out of view, we require that an intersection occur outside of the distance a particle

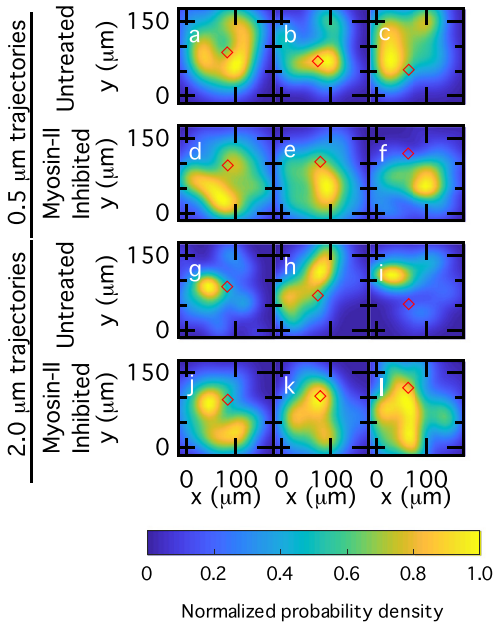

Fig. 5. Spatial probability density of intersections between vectors extended from (a-f) 0.5 and (g-l) 2.0 µm probe particles in pericellular regions around (a-c and g-i) untreated and (d-f and j-l) myosin-II inhibited hMSCs. Probability is normalized by the maximum probability in each sample and represented by a color bar with yellow and green representing high probability and blue representing low probability. The initial cell center is indicated by a diamond. (a-c) and (g-i) are measurements of the same pericellular region around an untreated hMSC and (d-f) and (j-l) are from the same pericellular region around a myosin-II inhibited hMSC. Data are taken (a, g) 5, (b, h) 27, (c, i) 43, (d, j) 5, (e, k) 21 and (f, l) 44 min after bi-disperse measurements are begun in that pericellular region. (a-f) For 0.5 µm particles, intersections occur throughout the field of view indicating that probe particles are undergoing Brownian motion. (g-i) Pericellular regions measured around untreated hMSCs with 2.0 µm particles, have intersections concentrated in specific regions in the field of view indicating that these particles are being pulled towards a force center. (j-l) Pericellular regions measured around myosin-II inhibited hMSCs with 2.0 µm particles have trajectory intersections randomly dispersed throughout the field indicating that their movement is Brownian. (For interpretation of the references to color in this figure legend, the reader is referred to the web version of this article.)

would diffuse in water during our data acquisition window. This ensures that we are not allowing a particle to intersect with itself. Details of this calculation are outlined in the Supplementary Material. Outside of this range, we identify the intersection with the shortest summed distance between the point of intersection and the initial locations of the two particles whose vectors make that intersection. The average vector would measure directed particle motion if a particle is stuck in the network and is being pulled by cellular traction. If particles are being pulled, this intersection will likely occur where force is being generated. For samples where only Brownian motion occurs, calculated vectors will point in random directions.

The concentration of intersections is used to identify force centers. Fig. 5 shows representative images of spatial probability density of intersections of 0.5 and 2.0 µm particles in a pericellular region around either an untreated or myosin-II inhibited hMSC. Color is used to represent the normalized probability density of intersections in the field of view. This two-dimensional probability density function (PDF) is calculated from particle intersections using a kernel smoothing function. The probability is normalized by the maximum probability in each image to enable side-by-side comparisons that are not biased by the number of particles in the collected data. A high probability, represented by yellow, indicates that intersections are concentrated in this region and it is a force center.

Intersection of 0.5 µm particles in pericellular regions around untreated hMSCs and myosin-II inhibited hMSCs are shown in Fig. 5a-c and Fig. 5d-f, respectively. In each pericellular region there is a maxima, but on average these maxima cover a large area of the image and a high probability of intersections is measured throughout the image. This large spread in the PDF indicates that 0.5 µm particles are intersecting across the entire image meaning that the particle motion is Brownian and not directed. The PDFs for both the untreated (Fig. 5a-c) and myosin-II inhibited 0.5 µm particle intersections (Fig. 5d-f) show similar spreads in particle intersections indicating that this length scale is not affected by cellularly applied forces.

PDFs for 2.0 µm particle intersections in pericellular regions around untreated and myosin-II inhibited hMSCs are shown in Fig. 5g-i and Fig. 5j-l, respectively. PDFs calculated for pericellular regions around untreated hMSCs show small regions of concentrated intersections, Fig. 5g-i. This indicates that probe particles are being pulled to small regions in the field of view likely due to the hMSC applying force on the network during migration. This occurs after the scaffold has been partially degraded and the 2.0 µm particles are trapped in the porous network, which is displaced and pulled towards the region where force is applied. In contrast to the intersections in the pericellular regions around untreated hMSCs, 2.0 µm particle intersections around myosin-II inhibited hMSCs are occurring randomly throughout the pericellular region, shown in Fig. 5j-l, and are similar to the PDFs calculated for 0.5 µm particles. This indicates that 2.0 µm particles around myosin-II inhibited cells are not directed and are instead undergoing Brownian motion. The transition from small, high probability regions to an increased spread in the intersection locations shows that cytoskeletal tension is responsible for directed particle motion on these larger length scales.

The results shown in Fig. 5 provide a map of particle intersections in a single pericellular region. To further quantify these intersections and provide a measure of force centers in all pericellular regions, we calculate the average nearest neighbor separation distance between intersections, $\langle N.N.\delta \rangle$. $\langle N.N.\delta \rangle$ is affected by the number of particles in the sample. As the number of particles increases, the number of intersections increases. This will result in a lower $\langle N.N.\delta \rangle$ even when particle trajectories are random. To account for this, we determine how $\langle N.N.\delta \rangle$ changes when an increasing number of random uniformly distributed points, N_{int}, are placed in the field of view. An equation describing how $\langle N.N.\delta \rangle$ changes with respect to N_{int} is then fit. For each sample, the calculated $\langle N.N.\delta \rangle$ for particles is normalized by the value from the equation. Normalized $\langle N.N.\delta \rangle$ values equal to 1 indicate that the intersections among particles are uniformly and randomly distributed. Values less than 1 indicate that the intersections are more concentrated. Details of how $\langle N.N.\delta \rangle$ varies with respect to N_{int} are given in the Supplementary Material (Section S3).

Fig. 6 shows the smoothed probability distribution function of the normalized $\langle N.N.\delta \rangle$ for 0.5 and 2.0 µm particles for all cells on each of the 3 days post-encapsulation. When holding post-encapsulation day and particle size constant while changing treatment condition, no significance is measured. When myosin-II is inhibited, the hMSC must adopt a different migratory strategy which may not impact $\langle N.N.\delta \rangle$. However we do measure differences when varying particle size, post-encapsulation day and when comparing pericellular region data with water samples.

We will begin by discussing how $\langle N.N.\delta \rangle$ varies between particle sizes while keeping treatment condition and post-encapsulation day constant. In the pericellular region around untreated hMSCs, Fig. 6a-c, we measure a statistically significant lower value of $\langle N.N.\delta \rangle$ for 2.0 µm particles than $\langle N.N.\delta \rangle$ for 0.5 µm particles on all days regardless of treatment condition. This shows that the larger 2.0 µm particles have more directed motion re-

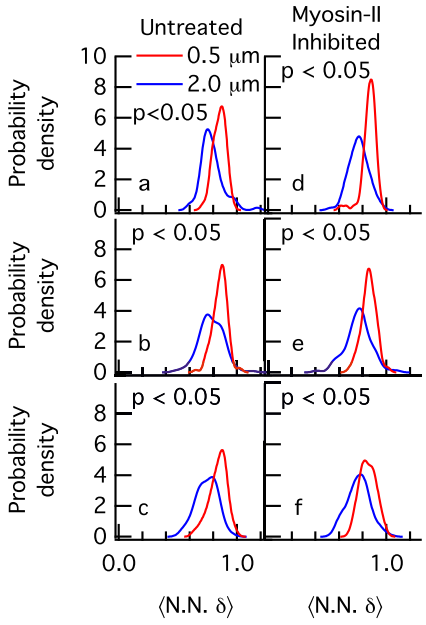

Fig. 6. The distribution of the average nearest neighbor distance, $\langle N.N.\delta \rangle$, for pericellular regions around (a-c) untreated and (d-f) myosin-II inhibited hMSCs on day (a and d) 1, (b and e) 2 and (c and f) 3 post-encapsulation. Lower values of $\langle N.N.\delta \rangle$ indicate intersections are closer together while high values indicate a more uniform distribution of intersections throughout the field of view. For all measurements, 2.0 μm particle $\langle N.N.\delta \rangle$ is significantly lower than $\langle N.N.\delta \rangle$ calculated with 0.5 μm particles ($p < 0.05$).

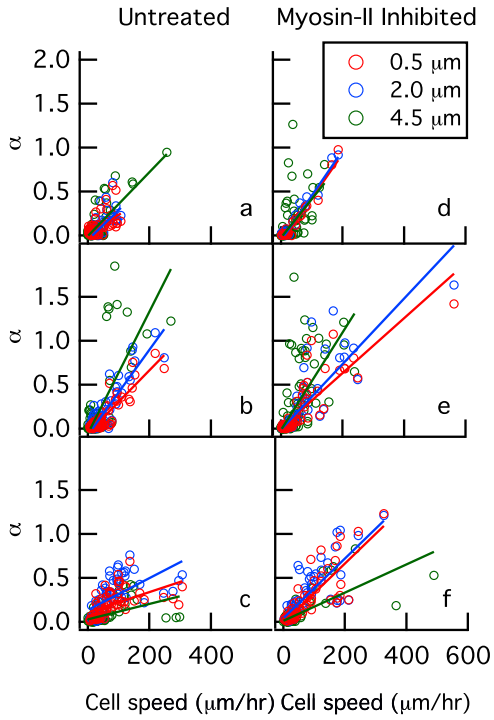

Fig. 7. Correlations between cell speed and pericellular rheology, α, for (a-c) untreated and (d-f) myosin-II inhibited hMSCs on day (a and d) 1, (b and e) 2 and (c and f) 3 post-encapsulation. The line of best fit is shown. These correlations relate the rheology of the material to the measured cell behavior. A table of significance p-values, from comparison of the slopes of each correlation is provided in the Supplementary Material, Table S1.

gardless of cellular treatment. We hypothesize that in the pericellular regions around untreated hMSCs, this is quantifying 2.0 μm particles intersecting at force centers, as we see in Fig. 5g-i. We also measure on average that $\langle N.N.\delta \rangle$ is similar in pericellular regions around myosin-II inhibited hMSCs. Here, we hypothesize this is due to degradation of the scaffold occurring at smaller length scales first resulting in lower diffusivity of these larger particles.

When holding treatment condition and particle size constant and comparing measurements made on different days, we see no significant changes over the course of the experiment for 0.5 μm particle $\langle N.N.\delta \rangle$ in pericellular regions around untreated hMSCs. This is likely because this length scale is measuring enzymatic scaffold degradation in the pericellular region which occurs throughout our observation window. This is also true for 0.5 μm particle $\langle N.N.\delta \rangle$ in myosin-II inhibited populations with the exception of day 1 and day 3 where we measure a statistically different $\langle N.N.\delta \rangle$ distribution. The day 3 distribution has a lower peak and is broader than both the day 1 and 2 distributions, reflecting the variety of microenvironments created by the hMSC during later stage remodeling and relatively high motility. When comparing $\langle N.N.\delta \rangle$ measured for 2.0 μm particles in pericellular regions around untreated hMSCs, statistically significant differences only occur when comparing day 3 to days 1 and 2. The mean $\langle N.N.\delta \rangle$ is lowest for 2.0 μm particles on day 3 indicating that these particles are intersecting the closest on this day, likely due to cytoskeletal tension. By day 3, hMSCs are exerting forces on the network to move rapidly and the pericellular region has been degraded. No significance is measured by 2.0 μm particle $\langle N.N.\delta \rangle$ when comparing pericellular regions around myosin-II inhibited hMSCs on different days. This is likely because without hMSCs pulling on the network, only cell-secreted MMPs can remodel the network structure and a significant amount of degradation must occur for 2.0 μm particles to move freely.

When comparing each particle size in each treatment condition with the measured $\langle N.N.\delta \rangle$ for water, we measure how the pericellular region differs from a purely diffusive environment with no length scale dependent structure. The distribution for water can be found in the Supplementary Material (Figure S11). The $\langle N.N.\delta \rangle$ measured for 0.5 μm particles in water is very narrow, resulting in statistically significant differences when compared to the $\langle N.N.\delta \rangle$ measured for 0.5 μm particles for pericellular regions around untreated hMSCs on day 3 and pericellular regions around myosin-II inhibited hMSCs on days 2 and 3. This is likely due to the heterogeneous microenvironments probed by the 0.5 μm particles on these later days when significant remodeling has occurred. This increased remodeling flattens and broadens the $\langle N.N.\delta \rangle$ relative to the water distribution resulting in a statistically significant difference. Statistical significance is always measured for $\langle N.N.\delta \rangle$ for 2.0 μm particles in pericellular regions when comparing with water regardless of treatment condition or day. This is likely because the movement of these large particles are significantly changed by both the structure of the material in the pericellular region and hMSC-mediated remodeling, neither of which are present in the water sample.

Together, Figs. 4, 5 and 6 show that hMSCs use cytoskeletal tension during migration to remodel the pericellular region on the 2.0 μm length scale. Since this indicates that length scale dependent rheology of the pericellular region is an important factor in cell motility, we correlate the rheology of the pericellular region with cell speed. This correlates the state of the material measured at different length scales with the ability for a cell to effectively migrate through that material. Fig. 7 shows the results of these correlations. The slope, m, of each correlation is determined and compared for significance against other measurements on that day. A full table of slope values is provided in Table 1. A table containing statistical significance for slope comparisons is provided in Table S1.

On day 1 post-encapsulation, Fig. 7a and d, hMSCs are beginning to remodel their microenvironment through MMP secretions

Table 1
Values of the slope, m, calculated from fitting the value of α versus cell speed (data plotted in Fig. 7). The values are given as the slope plus or minus the standard error.

		Untreated Slope ($\times 10^3$)	Myosin-II Inhibited Slope ($\times 10^3$)
Day 1	0.5 μm	2.1 ± 0.4	5.0 ± 0.2
	2.0 μm	3.4 ± 0.4	5.1 ± 0.2
	4.5 μm	3.6 ± 1.0	4.4 ± 0.5
Day 2	0.5 μm	3.6 ± 0.2	3.1 ± 0.2
	2.0 μm	4.9 ± 0.2	3.7 ± 0.3
	4.5 μm	7.0 ± 0.5	5.6 ± 0.5
Day 3	0.5 μm	1.2 ± 0.2	3.4 ± 0.3
	2.0 μm	1.8 ± 0.3	3.4 ± 0.3
	4.5 μm	0.9 ± 0.2	1.6 ± 0.2

and are limited to lower cell speeds and α values. The slopes of these correlations are only statistically significant ($p < 0.05$) between the 0.5 and 2.0 μm particles around untreated hMSCs. The slope is smaller for the 0.5 μm particles, indicating that less remodeling needs to occur on this length scale than on the 2.0 μm length scale to enable the same cell speeds. There is no significant difference measured as a function of length scale for myosin-II inhibited hMSCs. When comparing between the untreated and myosin-II inhibited hMSCs, we measure that the slope of 0.5 μm particles of pericellular regions around untreated cells is significantly lower than any length scale measured around myosin-II inhibited hMSCs. Again this indicates that untreated hMSCs require less pericellular remodeling on the 0.5 μm length scale to achieve the same motility. The slope measured by 2.0 μm particles around untreated hMSCs is also significantly smaller than the slopes measured by 0.5 and 2.0 μm particles around myosin-II inhibited hMSCs. The slope measured by 4.5 μm particles around untreated hMSCs is not statistically significant when compared to slopes around myosin-II inhibited hMSCs at any length scale. At this larger length scale, significant enzymatic degradation needs to occur for 4.5 μm particles to become motile. On day 1 post-encapsulation, hMSCs have not had enough time to degrade the scaffold resulting in low values of α for these particles.

Fig. 7b and e show correlations between cell speed and scaffold rheology 2 days post-encapsulation. Measurements of untreated and myosin-II inhibited hMSCs and their pericellular regions now show significant length scale dependence, evidenced by the curves separating in Fig. 7b and e. For untreated cells, measurements of the pericellular region with 0.5 μm particles is significantly lower than the larger length scales. This indicates that on the 0.5 μm length scale there is less movement of the probe particles for the same cell motility measured at larger length scales. hMSCs are actively pulling on the network to remodel larger length scales, leading to a significant increase in m with particle size. On day 2, the scaffold has been partially degraded and the movement of the 2.0 and 4.5 μm particles is still restricted by the remaining pore structure. This results in these particles having directed motion when tension is applied to the network by the hMSC. This directed motion results in a higher α value for the larger particles while smaller particles can roll through the porous degraded scaffold.

For mysoin-II inhibited hMSCs 2 days post-encapsulation, no significant difference is measured between m values characterized with 0.5 and 2.0 μm particles. These results are similar to the measurement of $\Delta\alpha$ in Fig. 4. The difference in α decreases when myosin-II is inhibited, indicating that there is little to no difference in scaffold remodeling between the 0.5 and 2.0 μm length scales. For myosin-II inhibited hMSCs, the slope measured by 4.5 μm particles is significantly larger than the 0.5 and 2.0 μm particle measurements. These larger length scales are on the order of the degradation length scale required for effective cell migration [2]. Finally, we measure a significant decrease in the slope of 0.5 and 2.0 μm particles around myosin-II inhibited hMSCs when compared to 2.0 μm particles around untreated hMSCs. This indicates that there is less remodeling on the 0.5 and 2.0 μm length scale when myosin-II is inhibited giving further evidence that cytoskeletal tension is remodeling the scaffold at the 2.0 μm length scale around untreated hMSCs. The slope correlating cell motility with pericellular rheology measured by 4.5 μm particles around untreated hMSCs is significantly higher than any measured length scale in the myosin-II inhibited hMSC pericellular regions. This is again likely due to the increased degradation from the combination of cytoskeletal tension and MMP secretions by untreated hMSCs.

On day 3 post-encapsulation, Fig. 7c and f, the values of m are lower than previous days for all untreated hMSCs and the correlation for the 4.5 μm length scale for myosin-II inhibited cells. For untreated hMSCs, this decrease in m is because 3 days post-encapsulation hMSCs have remodeled the pericellular region and are motile. Since the scaffold is being minimally remodeled on this day, the effects of cytoskeletal tension are small and the values of α are above the gel-sol transition but are no longer directed, which would result in $\alpha > 1$. Therefore, the slope is decreased because $\alpha < 1$ and cell speed increases. On this day, no significant difference is measured between the 0.5 and 2.0 μm particles. This is likely due to the increased degradation of the scaffold with pore sizes that are now larger than 2.0 μm particles enabling diffusion of these probes. When forces are applied to the network, these larger particles which would have been moved with the matrix on days 1 and 2, can now move through the degraded matrix as it is pulled and are therefore not measuring cytoskeletal tension during motility. Measurements for myosin-II inhibited hMSCs also have no significant difference between 0.5 and 2.0 μm slopes. No significant difference is measured on any day post-encapsulation around myosin-II inhibited cells, confirming that there is no length scale dependent rheological changes during cell-mediated enzymatic remodeling of the pericellular region. The value of m measured by 4.5 μm particles have the lowest slope for both conditions on this day. By day 3, only 4.5 μm particles still trapped in the gel scaffold remain in the field of view. In degraded regions of the scaffold, these particles have settled out under gravity. Since the available particles for MPT measurements are embedded in the gel, the measurement is biased towards lower α values, leading to low values of m on day 3 for both treatment conditions. We also measure a statistically significant reduction in the number of 4.5 μm particles available for microrheological measurements on day 3 as compared to previous days. We will not discuss 4.5 μm particles further due to the lack of statistics in the measurement.

Finally, when comparing the untreated and myosin-II inhibited hMSC remodeling and motility 3 days post-encapsulation, we measure a significantly lower value of m around untreated hMSCs for both 0.5 and 2.0 μm particles. This indicates that around untreated hMSCs, there is less scaffold degradation and remodeling for the same cell speed than for myosin-II inhibited hMSCs. This indicates that there is increased degradation of the scaffold, which would result in higher α values, measured around myosin-II inhibited hMSCs. Additionally, myosin-II inhibited hMSCs have also been measured to have a significant decrease in cell speed when compared to untreated hMSCs [6]. This would also lower the value of m for myosin-II inhibited cells.

Overall, the correlations between α and cell speed, Fig. 7, show the importance of length scale dependent rheology in enabling cell motility, a basic cellular process. We determine that cytoskeletal tension remodels the 2.0 μm length scale of a partially degraded scaffold. In these scaffolds, the 2.0 μm particles are measuring cytoskeletal tension and are being pulled with the network. 0.5 μm particles are measuring a more open porous net-

work and can slip through the network when force is applied. 4.5 μm particles also measure cytoskeletal tension applied to the network. Combining these correlations with measurements of $\Delta\alpha$ show that the difference in 0.5 and 2.0 μm particle mobility is removed when cytoskeletal tension is inhibited, Fig. 4. Additionally, the identification of force centers in Figs. 5 and 6 indicate that hMSCs use different strategies to remodel the pericellular region at different length scales. Namely, enzymatic degradation remodels the 0.5 μm length scale while cytoskeletal tension remodels the 2.0 and 4.5 μm length scales. This leads to heterogeneous environments with specifically engineered rheology that enables basic cellular processes.

4. Conclusions

This work uses bi-disperse MPT and MPT to characterize the length scale dependent rheology of the pericellular region of a migrating hMSC. During remodeling, we measure significant differences across length scales, quantified by $\Delta\alpha$, with larger length scales being more remodeled than smaller length scales. When cytoskeletal tension is inhibited, all length scales are remodeled similarly, indicating that larger length scales are remodeled by cytoskeletal tension. To further characterize the impact of cytoskeletal tension on the surrounding material, intersections between projected particle vectors are identified. These show that smaller particles are not directed by cellularly applied forces while larger particles are. When myosin-II is inhibited, intersections remain random for 0.5 and 2.0 μm particles. This confirms that this larger length scale is remodeled primarily by tension. $\langle N.N.\delta \rangle$ quantifies how material on each length scale is modified on different days post-encapsulation indicating that larger length scales are more directed and that the distribution of $\langle N.N.\delta \rangle$ changes as remodeling progresses. Finally correlations between the state of the material and cell motility are measured on each length scale. Larger length scales require more remodeling for a given cell speed than smaller length scales.

This work characterizes changes in length scale dependent rheology in the pericellular region, building on previous work which used traditional MPT [6–9]. These results show that hMSCs remodel their microenvironment by changing material properties on different length scales using different mechanisms of scaffold degradation. MMPs degrade the pericellular region on small length scales resulting in the increase in pore structure. Cytoskeletal tension remodels larger length scales through the application of force on the network. Additionally, this work contributes to the growing body of work emphasizing the importance of length scale in the design and functionality of biomaterials. Characterizing these unique, heterogeneous pericellular regions are key to enabling the design of new materials that can be instructive to encapsulated cells by mimicking these microenvironments to enhance migration and cell delivery after implantation.

Declaration of Competing Interest

The authors declare that they have no known competing financial interests or personal relationships that could have appeared to influence the work reported in this paper.

Acknowledgements

Funding for this work was provided by the National Science Foundation (NSF) under Grant No. CBET-1751057. The authors would like to thank Timothy Hawes for helpful discussions regarding data analysis for this work and Professor Jennifer Leight for discussions about blebbistatin's effect on MMP activity.

Supplementary material

Supplementary material associated with this article can be found, in the online version, at doi:10.1016/j.actbio.2020.11.048.

References

[1] E. Eggenhofer, F. Luk, M.H. Dahlke, M.J. Hoogduijn, The life and fate of mesenchymal stem cells, Front. Immunol. 5 (2014) 148.
[2] K. Wolf, M.T. Lindert, M. Krause, S. Alexander, J.T. Riet, A.L. Willis, R.M. Hoffman, C.G. Figdor, S.J. Weiss, P. Friedl, Physical limits of cell migration: control by ECM space and nuclear deformation and tuning by proteolysis and traction force, J Cell Biol 201 (2013) 1069–1084.
[3] A. Seidi, M. Ramalingam, I. Elloumi-Hannachi, S. Ostrovidov, A. Khademhosseini, Gradient biomaterials for soft-to-hard interface tissue engineering, Acta Biomater. 7 (2011) 1441–1451.
[4] R.T. Justin, A.J. Engler, Stiffness gradients mimicking in vivo tissue variation regulate mesenchymal stem cell fate, PLoS ONE 6 (2011) e15978.
[5] S. Cosson, S.A. Kobel, M.P. Lutolf, Capturing complex protein gradients on biomimetic hydrogels for cell-based assays, Adv. Funct. Mater. 19 (2009) 3411–3419.
[6] K.M. Schultz, K.A. Kyburz, K.S. Anseth, Measuring dynamic cell-material interactions and remodeling during 3d human mesenchymal stem cell migration in hydrogels, Proceedings of the National Academy of Sciences 112 (2015) E3757–E3764.
[7] M. Daviran, S.M. Longwill, J.F. Casella, K.M. Schultz, Rheological characterization of dynamic remodeling of the pericellular region by human mesenchymal stem cell-secreted enzymes in well-defined synthetic hydrogel scaffolds, Soft Matter. 14 (2018) 3078–3089.
[8] M. Daviran, H.S. Caram, K.M. Schultz, Role of cell-mediated enzymatic degradation and cytoskeletal tension on dynamic changes in the rheology of the pericellular region prior to human mesenchymal stem cell motility, ACS biomaterials science & engineering 4 (2018) 468–472.
[9] M. Daviran, K.M. Schultz, Characterizing the dynamic rheology in the pericellular region by human mesenchymal stem cell re-engineering in peg-peptide hydrogel scaffolds, Rheol. Acta (2019) 1–17.
[10] M.S. Mazzeo, T. Chai, M. Daviran, K.M. Schultz, Characterization of the kinetics and mechanism of degradation of human mesenchymal stem cell-laden poly (ethylene glycol) hydrogels, ACS Applied Bio Materials 2 (2018) 81–92.
[11] M. Daviran, J. Catalano, K.M. Schultz, Determining how human mesenchymal stem cells change their degradation strategy in response to microenvironmental stiffness, Biomacromolecules (2020).
[12] P. Friedl, K. Wolf, Plasticity of cell migration: a multiscale tuning model, J. Cell Biol. 188 (2010) 11–19.
[13] W.R. Legant, J.S. Miller, B.L. Blakely, D.M. Cohen, G.M. Genin, C.S. Chen, Measurement of mechanical tractions exerted by cells in three-dimensional matrices, Nat. Methods 7 (2010) 969–971.
[14] M. Lutolf, J. Lauer-Fields, H. Schmoekel, A.T. Metters, F. Weber, G. Fields, J.A. Hubbell, Synthetic matrix metalloproteinase-sensitive hydrogels for the conduction of tissue regeneration: engineering cell-invasion characteristics, Proceedings of the National Academy of Sciences 100 (2003) 5413–5418.
[15] J. Roether, S. Bertels, C. Oelschlaeger, M. Bastmeyer, N. Willenbacher, Microstructure, local viscoelasticity and cell culture suitability of 3d hybrid ha/collagen scaffolds, PLoS ONE 13 (2018) e0207397.
[16] J. Hafner, D. Grijalva, A. Ludwig-Husemann, S. Bertels, L. Bensinger, A. Raic, J. Gebauer, C. Oelschlaeger, M. Bastmeyer, K. Bieback, et al., Monitoring matrix remodelling in the cellular microenvironment using microrheology for complex cellular systems, Acta Biomater. (2020).
[17] L. Pavlovsky, J.G. Younger, M.J. Solomon, In situ rheology of staphylococcus epidermidis bacterial biofilms, Soft Matter 9 (2013) 122–131.
[18] L. Han, A.J. Grodzinsky, C. Ortiz, Nanomechanics of the cartilage extracellular matrix, Annu. Rev. Mater. Res. 41 (2011) 133–168.
[19] R.C. Arevalo, J.S. Urbach, D.L. Blair, Size-dependent rheology of type-i collagen networks, Biophys. J. 99 (2010) L65–L67.
[20] B.D. Fairbanks, M.P. Schwartz, A.E. Halevi, C.R. Nuttelman, C.N. Bowman, K.S. Anseth, A versatile synthetic extracellular matrix mimic via thiol-norbornene photopolymerization, Adv. Mater. 21 (2009) 5005–5010.
[21] G. Raeber, M. Lutolf, J. Hubbell, Molecularly engineered peg hydrogels: a novel model system for proteolytically mediated cell migration, Biophys. J. 89 (2005) 1374–1388.
[22] M.W. Tibbitt, K.S. Anseth, Hydrogels as extracellular matrix mimics for 3d cell culture, Biotechnol. Bioeng. 103 (2009) 655–663.
[23] S.J. Bryant, K.S. Anseth, Hydrogel properties influence ECM production by chondrocytes photoencapsulated in poly (ethylene glycol) hydrogels, Journal of Biomedical Materials Research: An Official Journal of The Society for Biomaterials and The Japanese Society for Biomaterials 59 (2002) 63–72.
[24] O. Chaudhuri, L. Gu, D. Klumpers, M. Darnell, S.A. Bencherif, J.C. Weaver, N. Huebsch, H.-p. Lee, E. Lippens, G.N. Duda, et al., Hydrogels with tunable stress relaxation regulate stem cell fate and activity, Nat. Mater. 15 (2016) 326.
[25] A.J. Engler, S. Sen, H.L. Sweeney, D.E. Discher, Matrix elasticity directs stem cell lineage specification, Cell 126 (2006) 677–689.
[26] D. Dikovsky, H. Bianco-Peled, D. Seliktar, Defining the role of matrix compliance and proteolysis in three-dimensional cell spreading and remodeling, Biophys. J. 94 (2008) 2914–2925.

[27] C.R. Nuttelman, M.C. Tripodi, K.S. Anseth, Synthetic hydrogel niches that promote hmsc viability, Matrix Biol. 24 (2005) 208–218.
[28] K.M. Schultz, K.S. Anseth, Monitoring degradation of matrix metalloproteinases-cleavable peg hydrogels via multiple particle tracking microrheology, Soft Matter 9 (2013) 1570–1579.
[29] J. Patterson, J.A. Hubbell, Enhanced proteolytic degradation of molecularly engineered peg hydrogels in response to mmp-1 and mmp-2, Biomaterials 31 (2010) 7836–7845.
[30] C. Yang, F.W. DelRio, H. Ma, A.R. Killaars, L.P. Basta, K.A. Kyburz, K.S. Anseth, Spatially patterned matrix elasticity directs stem cell fate, Proceedings of the National Academy of Sciences 113 (2016) E4439–E4445.
[31] K.A. Kyburz, K.S. Anseth, Three-dimensional hmsc motility within peptide–functionalized peg-based hydrogels of varying adhesivity and crosslinking density, Acta Biomater. 9 (2013) 6381–6392.
[32] H. Nagase, R. Visse, G. Murphy, Structure and function of matrix metalloproteinases and timps, Cardiovasc. Res. 69 (2006) 562–573.
[33] J.L. West, J.A. Hubbell, Polymeric biomaterials with degradation sites for proteases involved in cell migration, Macromolecules 32 (1999) 241–244.
[34] J.L. Leight, D.L. Alge, A.J. Maier, K.S. Anseth, Direct measurement of matrix metalloproteinase activity in 3d cellular microenvironments using a fluorogenic peptide substrate, Biomaterials 34 (2013) 7344–7352.
[35] D.A. Lauffenburger, A.F. Horwitz, Cell migration: a physically integrated molecular process, Cell 84 (1996) 359–369.
[36] S.K. Mitra, D.A. Hanson, D.D. Schlaepfer, Focal adhesion kinase: in command and control of cell motility, Nat. Rev. Mol. Cell Biol. 6 (2005) 56.
[37] N.Q. Balaban, U.S. Schwarz, D. Riveline, P. Goichberg, G. Tzur, I. Sabanay, D. Mahalu, S. Safran, A. Bershadsky, L. Addadi, et al., Force and focal adhesion assembly: a close relationship studied using elastic micropatterned substrates, Nat. Cell Biol. 3 (2001) 466.
[38] E.M. Furst, T.M. Squires, Microrheology, Oxford University Press, 2017.
[39] K.M. Schultz, E.M. Furst, Microrheology of biomaterial hydrogelators, Soft Matter 8 (2012) 6198–6205.
[40] T.G. Mason, Estimating the viscoelastic moduli of complex fluids using the generalized stokes-einstein equation, Rheol. Acta 39 (2000) 371–378.
[41] T.M. Squires, T.G. Mason, Fluid mechanics of microrheology, Annu. Rev. Fluid Mech. 42 (2010).
[42] J.C. Crocker, B.D. Hoffman, Multiple-particle tracking and two-point microrheology in cells, Methods Cell Biol. 83 (2007) 141–178.
[43] T.A. Waigh, Microrheology of complex fluids, Rep. Prog. Phys. 68 (2005) 685.
[44] J.A. McGlynn, N. Wu, K.M. Schultz, Multiple particle tracking microrheological characterization: fundamentals, emerging techniques and applications, J. Appl. Phys. 127 (2020) 201101.
[45] T. Mason, K. Ganesan, J.V. Zanten, D. Wirtz, S. Kuo, Particle tracking microrheology of complex fluids, Phys. Rev. Lett. 79 (1997) 3282.
[46] T.G. Mason, D. Weitz, Optical measurements of frequency-dependent linear viscoelastic moduli of complex fluids, Phys. Rev. Lett. 74 (1995) 1250.
[47] M.D. Wehrman, S. Lindberg, K.M. Schultz, Multiple particle tracking microrheology measured using bi-disperse probe diameters, Soft Matter 14 (2018) 5811–5820.
[48] B.D. Fairbanks, M.P. Schwartz, C.N. Bowman, K.S. Anseth, Photoinitiated polymerization of peg-diacrylate with lithium phenyl-2, 4, 6-trimethylbenzoylphosphinate: polymerization rate and cytocompatibility, Biomaterials 30 (2009) 6702–6707.
[49] C.N. Bowman, C.J. Kloxin, Toward an enhanced understanding and implementation of photopolymerization reactions, AIChE J. 54 (2008) 2775–2795.
[50] M.W. Tibbitt, A.M. Kloxin, L.A. Sawicki, K.S. Anseth, Mechanical properties and degradation of chain and step-polymerized photodegradable hydrogels, Macromolecules 46 (2013) 2785–2792.
[51] M. Valentine, Z. Perlman, M. Gardel, J.H. Shin, P. Matsudaira, T. Mitchison, D. Weitz, Colloid surface chemistry critically affects multiple particle tracking measurements of biomaterials, Biophys. J. 86 (2004) 4004–4014.
[52] J. Leight, Private communication (2020).
[53] J.C. Crocker, D.G. Grier, Methods of digital video microscopy for colloidal studies, J. Colloid Interface Sci. 179 (1996) 298–310.
[54] T. Savin, P.S. Doyle, Static and dynamic errors in particle tracking microrheology, Biophys. J. 88 (2005) 623–638.
[55] J.C. Crocker, E.R. Weeks, Particle tracking using idl, 2011, URl http://www.physics.emory.edu/faculty/weeks//idl/index.html.
[56] F.J. Massey Jr, The kolmogorov-smirnov test for goodness of fit, J. Am. Stat. Assoc. 46 (1951) 68–78.
[57] M.D. Bond, H.E.V. Wart, Characterization of the individual collagenases from clostridium histolyticum, Biochemistry 23 (1984) 3085–3091.
[58] H.H. Winter, F. Chambon, Analysis of linear viscoelasticity of a crosslinking polymer at the gel point, J. Rheol. (N Y N Y) 30 (1986) 367–382.
[59] M.D. Wehrman, S. Lindberg, K.M. Schultz, Quantifying the dynamic transition of hydrogenated castor oil gels measured via multiple particle tracking microrheology, Soft Matter 12 (2016) 6463–6472.
[60] T. Larsen, K. Schultz, E.M. Furst, Hydrogel microrheology near the liquid-solid transition, Korea-Australia Rheology Journal 20 (2008) 165–173.
[61] T.H. Larsen, E.M. Furst, Microrheology of the liquid-solid transition during gelation, Phys. Rev. Lett. 100 (2008) 146001.
[62] H. Winter, Can the gel point of a cross-linking polymer be detected by the G′–G″ crossover? Polymer Engineering & Science 27 (1987) 1698–1702.
[63] D. Adolf, J. Martin, Time-cure superposition during crosslinking, Macromolecules 23 (1990) 3700–3704.
[64] M. Vicente-Manzanares, X. Ma, R.S. Adelstein, A.R. Horwitz, Non-muscle myosin ii takes centre stage in cell adhesion and migration, Nat. Rev. Mol. Cell Biol. 10 (2009) 778–790.
[65] R. Aguilar-Cuenca, A. Juanes-García, M. Vicente-Manzanares, Myosin ii in mechanotransduction: master and commander of cell migration, morphogenesis, and cancer, Cell. Mol. Life Sci. 71 (2014) 479–492.